

# Finite Element Modeling of Lamb Wave Propagation in Anisotropic Hybrid Materials

MARKUS G. R. SAUSE<sup>1</sup>, MARVIN A. HAMSTAD<sup>2</sup> and SIEGFRIED HORN<sup>1</sup>

<sup>1</sup>University of Augsburg, Institute for Physics, Experimental Physics II, D-86135 Augsburg

<sup>2</sup>University of Denver, Department of Mechanical and Materials Engineering, Denver, CO, 80208

## Abstract

A finite element approach for modeling of acoustic emission sources and signal propagation in hybrid multi-layered plates is presented. Modeling results are validated by Laservibrometer measurements and comparison to calculated dispersion curves. We investigate hybrid plates as typically found in composite pressure vessels, composed of fiber reinforced polymers with arbitrary stacking sequences and attached metal or polymer materials. Hybrid plate thickness, the ratio between anisotropic and isotropic materials and material properties are varied. Lamb-wave propagation in a geometry representative of a pressure vessel is modeled. It is demonstrated, that acoustic emission sources in multi-layered structures can cause Lamb-waves superimposed by guided waves within the individual layers.

*Keywords: A. Layered structures, A. Polymer-matrix composites (PMCs), C. Finite element analysis (FEA), D. Acoustic emission*

## 1 INTRODUCTION

Within structural health monitoring applications, acoustic emission (AE) analysis is a technique, which is widely used [1]. AE signals in a solid originate from rapid microscopic displacements like active crack growth, dislocation movement or stick-slip friction. Detection of such microscopic processes can thus act as an early indicator of potential structural failure. Within the last decades fiber reinforced pressure vessels have been investigated extensively by AE monitoring to assess their integrity [2-4] or to predict their burst pressure [5, 6]. For sufficiently large thin-walled structures, acoustic signals propagate as guided waves. Although the mathematical description of signal propagation within an isotropic plate with traction-free boundaries was given by H. Lamb in 1917 [7], the numerical complexity inherent to the derived wave equations was still challenging until the increase of computational power at the end of the last century. Based on his ground-breaking research the type of guided wave found in thin plates has been named Lamb-waves. In principle, an infinite number of Lamb-wave modes can exist within a plate, one type with symmetric and one type with anti-symmetric motion with respect to the mid-plane of the plate. The types of modes faced most often in AE testing are the fundamental symmetric mode ( $S_0$ ) and anti-symmetric mode ( $A_0$ ),

often referred to as the extensional and flexural modes. However, higher-order modes can also be encountered in structures with sufficient thickness in the range above 3-5 mm, depending on the materials elastic properties.

While calculation of dispersive properties of Lamb-wave propagation in isotropic materials is nowadays found in various software packages, the calculation of Lamb-wave propagation in anisotropic media is still challenging for numerical methods. For AE testing of fiber reinforced materials the influence of Lamb-wave propagation is of a crucial nature, since the waves of a particular AE source may vary drastically in their appearance, depending on the propagation direction and the position of the source in the plate thickness. Thus the advanced interpretation of AE signals by modal AE analysis [8, 9] or pattern recognition techniques [10-17] has to consider the influence of Lamb-wave propagation. Despite some valuable numerical tools that allow for calculation of analytical solutions, finite element modeling was found to be a suitable tool to investigate signal propagation of guided waves [18-22]. In realistic structures hybrid materials are encountered many times. Typically, these are a combination of fiber reinforced materials with different fiber orientations and other materials, like metals or polymers. Under certain boundary conditions, these structures can be assumed to behave like a multi-layered plate.

In principle, numerical methods for analytical solutions to describe wave propagation in multi-layered structures were already given by Thomson and Haskell [23, 24]. However, many numerical challenges like the problem of ill-conditioned matrices as used for the transfer-matrix method had to be overcome. A good review on those developments is found in [25]. Also, analytical predictions for wave propagation in multi-layered structures are given by Mal and Kundu for the case of infinite half-spaces [26].

Compared to analytical solutions, a finite element approach to model Lamb-wave propagation in such structures is advantageous in two ways. First, arbitrary geometries can be implemented without substantial modifications of the chosen approach. In contrast, for analytical approaches, boundary conditions along with complex geometries are often difficult to implement. Second, 3-dimensional finite element modeling takes into account the boundary reflections of edges and additional interfaces, which are rarely adequately captured by analytical approaches. For the

special case of acoustic emission analysis one further advantage is the possibility to include in one model a geometrically complex source model and the detection process using a piezoelectric sensor [16, 21, 27].

In the present investigation we focus on the aspect of Lamb-wave propagation in multi-layered hybrid materials. Thus we compare the results of predictions from finite element modeling to measurement results using Laservibrometer measurements. Then we present results from various parameter studies using different layup configurations of multi-layered hybrid plates and compare the results to analytically calculated dispersion curve results. Finally the modeling approach is presented in application to a small pressure vessel with complex stacking sequence of individual fiber reinforced plies including a metallic liner material.

## 2 FINITE ELEMENT MODELING

The finite element simulation of Lamb-wave propagation is based on the calculation of stress-strain relationships in a specimen volume governed by the structural mechanics constitutive equation. Based on the principle of virtual work the finite element program COMSOL solves the partial differential equations for equilibrium conditions, expressed in global or local stress and strain components for an external stimulation (see e.g. [21, 22, 27, 28] for more details).

For linear elastic media, Hook's law is chosen as constitutive equation. In the general case for anisotropic media the elasticity tensor  $\vec{D}$  is a 6 x 6 matrix with 12 independent components. These can be reduced to five independent components for orthotropic materials like unidirectional carbon fiber reinforced plastics (CFRP) laminate. In the case of isotropic media, the number of independent components can be reduced to two and the elasticity tensor is defined by using e.g. Young's modulus  $E$  and Poisson's ratio  $\nu$ .

Figure 1 shows the model setup chosen for simulation of Lamb-wave propagation in multi-layered plate structures. A circular plate with 220 mm radius of different thicknesses between 1 mm and 4 mm is modeled using the xz-plane and yz-plane as symmetry planes. For all simulations on multi-layered plates, an AE dipole source is modeled at the position  $(x,y,z) = (0.0000,0.2000,0.5625 \times \text{thickness})$  mm within the plate. The dipole axis is oriented parallel to the y-

axis. As source function, a linear force pulse in y-direction with excitation time  $t_e$  and maximum force  $F_{\max}$  is used:

$$F(t) = \begin{cases} F_{\max} \cdot (t/t_e) & t \leq t_e \\ F_{\max} - F_{\max} \cdot (2(t-t_e)/t_e) & t_e < t \leq 1.5t_e \\ 0 & t > 1.5t_e \end{cases} \quad (1)$$

In combination with the symmetry condition at the xz-plane this corresponds to a dipole source with axis length 0.4 mm along the y-axis. The excitation time  $t_e$  was chosen to be 1  $\mu$ s with  $F_{\max}$  of 3 N. Lamb-waves are then evaluated as the out-of-plane displacement at designated points of the structure at a propagation distance of 100 mm in 0°, 45° and 90° direction as marked in figure 1.

The elastic properties of the materials investigated are summarized in table 1. As fiber reinforced materials, elastic properties of the HexPly prepreg system NCIM 913/35%/132/T800 (T800/913) were used. As isotropic materials, properties of aluminum alloy (AlMg3), high density polyethylene (HDPE) and titanium alloy (Ti-6Al-4V) are used as noted in table 1.

In order to model ply orientations different to 0° a rotated coordinate system was defined in COMSOL. Using the Z-X-Z Euler angles definition, a simulation of the 90° oriented ply was conducted with a rotated coordinate system setting the first Euler angle  $\alpha = 90^\circ$  as shown in figure 1. Other ply orientations were implemented in a similar fashion. For simulation of the different plies of the pressure vessel shown in figure 2, the curvature was taken into account by a rotation using the second Euler angle  $\beta$ . Ply orientations were then implemented by a subsequent rotation of the third Euler angle  $\gamma$ . The value of  $\beta$  depends on the (y,z)-coordinates and was calculated as a function of position using equation (2).

$$\beta(y, z) = \begin{cases} \arcsin\left(y/\sqrt{y^2 + z^2}\right) & z > 0 \\ \pi + \arcsin\left(y/\sqrt{y^2 + z^2}\right) & z \leq 0 \end{cases} \quad (2)$$

For the pressure vessel simulation, an AE dipole source is modeled at the position (x,y,z) = (0.0000,-0.2000,95.5416) mm within the plate. The dipole axis is oriented parallel to the y-axis. The source function is identical to those of the multi-layered plates.

In the following, all ply orientations are given relative to the 0° direction, subscript numbers refer to a repetition of the respective layer. A subscript “sym” outside the brackets indicates, that the complete layup is repeated once in reverse order to form a symmetric laminate.

In order to avoid reflections of the Lamb-waves at the plate edges, a low-reflection boundary condition was applied at the end of the plate as indicated in figure 1. These boundary conditions try to mimic an adjacent medium with identical acoustic impedance to avoid reflection of an incident acoustic wave. In order to match the acoustic impedance of the plies rotated by the Euler angle  $\alpha$ , the acoustic impedance  $Z$  tangential and normal to the boundaries was defined as function of the (x,y)-coordinates as follows:

$$Z_{\text{tangential}}(x, y) = \rho \cdot \sqrt{\frac{C_{12}}{\rho}} \quad (3a)$$

$$Z_{\text{normal}}(x, y) = \rho \cdot \left( \left( \sin \left( \left( \arcsin \left( \frac{x}{\sqrt{x^2 + y^2}} \right) \right) + \alpha \right) \cdot \sqrt{\frac{C_{11}}{\rho}} \right) + \left( \cos \left( \left( \arcsin \left( \frac{x}{\sqrt{x^2 + y^2}} \right) \right) + \alpha \right) \cdot \sqrt{\frac{C_{22}}{\rho}} \right) \right) \quad (3b)$$

While this concept was found to suppress reflection of the incident  $S_0$ -mode by more than 95.8 %, the incident  $A_0$ -mode was only suppressed by 45.7 % in the worst case. Since this reflection of the  $A_0$ -mode is not negligible for undisturbed observations of Lamb-wave propagation, the size of the plate was chosen to be large enough to avoid incoming reflections of this mode at the detection positions marked in figure 1.

All models were meshed with elements of 1 mm lateral size in the in-plane directions. Along the out-of-plane direction a minimum of one mesh element was chosen per layer modeled. All mesh elements are of quadratic geometry shape order. As temporal resolution, a step of 100 ns was chosen to calculate the first 100  $\mu$ s after signal excitation.

The sufficiency of these settings was investigated by calculation of reference signals with lower mesh element size and lower time step. Comparison between signals of the reference case and the

calculated signals is based on the coherence level of the signal within the frequency range of interest between 1 kHz and 1 MHz.

In frequency domain the coherence level  $\eta_{xy}$  of two signals  $x$  and  $y$  is defined as

$$\eta_{xy}(f) = \frac{|P_{xy}(f)|^2}{P_{xx}(f) \cdot P_{yy}(f)} . \quad (4)$$

$P_{xy}$  is the cross power density spectrum of the two signals  $x$  and  $y$ , while  $P_{xx}$  and  $P_{yy}$  are the power spectral densities of signals  $x$  and  $y$ , respectively. By definition, the coherence level is between zero and one.  $\eta_{xy} = 1$  indicates complete coherence of both signals,  $\eta_{xy} = 0$  indicates complete decoherence. To obtain the signals power density spectra, a FFT algorithm with binary length of 512 samples is used.

Two exemplary signals to compare are shown in figure 3-a. These are signals obtained from mesh sizes of 1 mm and of 0.5 mm but otherwise identical settings. Figure 3-b shows the calculated coherence level as a function of frequency. Since shorter wavelengths suffer from decreased mesh resolution first, a substantial decrease of the coherence level occurs above 1800 kHz. Within the frequency range of interest between 1 kHz and 1.5 MHz the coherence level of the two signals calculated with 1 mm mesh elements was  $\geq 0.981$  compared to the case for the mesh resolution of 0.5 mm. For lower mesh element sizes, the coherence level  $\eta_{xy} = 1$ .

To choose a sufficient temporal resolution we conducted similar investigations for the size of the time step. A systematic reduction from 100 ns to a 5 ns step size was made. For a step size below 5 ns the coherence level  $\eta_{xy}$  was always found to be 1 for frequencies below 2 MHz. For the time step of 100 ns chosen in the following the coherence level was found to be  $\geq 0.9705$  compared to the signal of the 5 ns time step. Hence, the chosen step size and mesh element size are suitable to obtain convergent results in the frequency range between 1 kHz and 1.5 MHz.

### 3 EXPERIMENTAL

For validation of the simulation approach, signals of pencil lead breaks on a 2 m x 1 m wide and 3 mm thick AlMg3 aluminum plate were used. Measurements were conducted using a Laservibrometer (model OFV-5000) with a displacement decoder unit (model DD-900). Pencil lead

breaks were applied at a distance of 100 mm to the point of detection. The signals were recorded using a data acquisition card (model PCI-2) with 40 dB preamplification and bandpass range between 20 kHz and 1 MHz. The measured out-of-plane displacement signal and the out-of-plane velocity signal are shown in figure 4-a and figure 4-b, respectively. For comparison a simulation of pencil lead breakage was conducted in a configuration as used experimentally. Simulation of pencil lead breakage as acoustic emission source follows the way of implementation published first in [29]. A linear ramp function with excitation time  $t_e$  and maximum force  $F_{\max}$  is used.

$$F(t) = \begin{cases} F_{\max} \cdot (t/t_e) & t \leq t_e \\ F_{\max} & t > t_e \end{cases} \quad (5)$$

The excitation time  $t_e$  of 1  $\mu\text{s}$  and maximum force  $F_{\max}$  for modeling of pencil lead breaks is based on our recent investigations [27, 28]. The resulting out-of-plane signal evaluated at the sensor positions was filtered by a 4<sup>th</sup> order Butterworth high-pass filter to take into account the experimentally used high-pass setting.

Within the range of scatter of the experimental signals the simulation results show good agreement to the Laservibrometer signals in shape and amplitude. The dominating mode observed for this configuration is the  $A_0$ -mode while the  $S_0$ -mode found at the initial part has only small amplitude. This is caused by the out-of-plane excitation of the pencil lead break source, which is a monopole source. While the small  $S_0$ -mode is still seen in the simulated signal (see inset in figure 4-a), the noise in the Laservibrometer signal inhibits precise detection of that part of the signal. This effect is also seen in the velocity signal shown in figure 4-b.

These experimental findings and the comparison between experimental signals and calculated signals in various composite geometries already reported in previous publications [16, 21, 27], allow to conclude, that the presented finite element approach is able to provide correct results for the investigation of Lamb-wave propagation in anisotropic hybrid materials.

## 4 RESULTS AND DISCUSSION

In the following, results of several numerical parameter studies are presented. The results are discussed using the signals obtained at various propagation angles as shown in figure 1. The

signals obtained are analyzed by Choi-Williams distributions and their time-frequency components are compared to dispersion curves calculated in an analytical approach.

First, the influence of the thickness ratio between layers of aluminum and CFRP is investigated. Next, the ratio is kept constant, and the thickness of the plate is varied. Further, the material properties of an isotropic thin layer are varied between aluminum, titanium and HDPE properties to assess their influence. Using aluminum as the material for the thin layer, the stacking sequence of the CFRP plies is varied to investigate the influence. Finally, we focus on a stacking sequence and geometry as typically found for a composite overwrapped pressure vessel.

#### **4.1 Thickness Ratio**

Using the results of homogeneous aluminum and pure T800/913 unidirectional CFRP as extreme values, a combination of both materials is investigated as a two layer system. The thickness ratio between aluminum and CFRP is systematically varied from 0 to 0.125 to 0.25 to 0.5 to 1 of the total thickness of 1 mm. Simulated signals shown in figures 5 are for an AE dipole source buried in the CFRP part with axis orientation along the y-axis, that is detected at 100 mm distance under 90° propagation angle on the top surface (composite side) of the plate. To identify particular Lamb-wave modes, the Choi-Williams distributions shown in figure 5 are superimposed by results of dispersion curve calculations following reference [22].

The separation in time of the  $S_0$ -mode and  $A_0$ -mode is observed strongest in pure CFRP and weakest in homogenous aluminum. The modes of the signal shown in figure 5-b are identified as symmetric and anti-symmetric motion relative to the midplane of the plate. While the match to the calculated dispersion curve of the  $A_0$ -mode of the hybrid plate is excellent, the agreement to the  $S_0$ -mode is less obvious. In addition to the barely visible  $S_0$ -mode of the hybrid plate, an additional propagation mode is found for an guided wave propagating in the CFRP layer. Therefore, the Lamb-wave propagation for this case seems to occur as a motion of the complete plate superimposed by an guided wave within one of the plate layers.

For varying ratio between aluminum and CFRP, a systematic transition of signal shape and propagation velocities is found. Similar to the  $S_0$ -mode the signal shape of the  $A_0$ -mode is changed continuously between the two extreme values of pure CFRP and pure aluminum, while the

amplitude is subject to a nonlinear transition. There is significant influence on the propagation velocity of the  $S_0$ -mode and the  $A_0$ -mode when the thickness ratio between aluminum and CFRP is changed. The values of the initial arrival velocities of the  $S_0$ -mode and the  $A_0$ -mode obtained from the simulation results are given in table 2.

The agreement between the simulated velocities and those obtained from the rule of mixture of the velocities of the pure materials indicate that the velocity of Lamb-wave propagation of the  $S_0$ -mode is governed by the average elastic properties of the materials involved. This is of particular interest for AE source localization approaches, that are based on the initial threshold crossing. A similar transition of propagation velocities is found for the  $A_0$ -mode. However, a direct application of the rule of mixture does not capture the changes in propagation velocity. This is due to the correlation of the  $A_0$ -mode velocity with the overall bending stiffness of the plate, which cannot be obtained from a direct rule of mixture calculation of the individual sound velocities of the materials involved.

Also, the ratio between anisotropic and isotropic seems to be the key factor for the changes in signal propagation. Thus for thickness ratios as typically faced for thin liner materials ( $< 0.125$  of the total thickness) the influence of the liner on signal propagation can assumed to be minimalistic.

#### **4.2 Plate thickness**

Because Lamb-wave formation and propagation is inevitably linked to the total thickness of the plate, the next step is an investigation of this factor of influence. The thickness ratio between aluminum and CFRP is kept constant at 0.5 of the total thickness. Simulated signals shown in figure 6 are for an buried AE dipole source with axis orientation along the y-axis detected at 100 mm distance under  $90^\circ$  propagation angle on the top surface (composite side) of the plate.

In contrast to the corresponding investigation with 1.00 mm thickness shown in figure 5-b, more than two Lamb-wave modes can be identified in the Choi-Williams distribution. For the 2.00 mm thickness, two propagation modes are found at the beginning of the signal. These again originate from a  $S_0$ -mode Lamb-wave of the hybrid plate and an additional guided wave propagating in the CFRP layer. The detected  $A_0$ -mode is caused by a respective motion of the hybrid plate, i.e. both layers. For the 4.00 mm thick plate shown in figure 6-b, even more propagation modes are

observed. The dominant propagation modes are identified as  $S_0$ -mode,  $S_1$ -mode,  $A_0$ -mode and  $A_1$ -mode of the hybrid plate. The guided wave in the CFRP layer (expected at around 225 kHz) is barely visible in the Choi-Williams distribution.

The unequal propagation within the hybrid plates is also seen in the signals detected under  $0^\circ$  propagation angle, as shown in figure 7. The comparison of the signal detected on the aluminum side (figure 7-a) and detected on the composite side (figure 7-b) demonstrates the distinct difference of the signals. While both signals exhibit the same intensity of the  $A_0$ -mode, the  $S_0$ -mode and  $S_1$ -mode yield much stronger intensities when detected on the CFRP side. On the Aluminum side an identification of the weak  $S_0$ -mode of the hybrid plate is almost impossible. This demonstrates that Lamb-wave propagation in such multi-layered plates can take place as motion of the complete plate, but also as a guided wave in only one of the layers.

#### **4.3 Elastic Properties of Liner Material**

In order to investigate the influence of liner materials in more detail, the thickness of the liner is kept constant at 0.125 mm, while the elastic properties of the liner are varied. The properties of the remaining 0.875 mm of the plate have T800/913 elastic properties. The thickness of the liner was chosen to reflect the typical conditions, where CFRP is used to carry the structural load and a metal or polymer is used to improve the electrical conductivity or decrease the permeability of CFRP [30, 31]. Figure 8 shows the signal detected on the top surface (composite side) at 100 mm distance at  $90^\circ$  and  $0^\circ$  propagation angles for the three liner materials investigated.

Overall, the signals are closer to the type of signal found for a pure T800/913 plate. Still, there is significant influence by the presence of the liner material. In particular, the type of liner material was found to affect the intensity of the  $S_0$ -mode and the  $A_0$ -mode.

Compared to the signal of pure CFRP the presence of a titanium liner is found to be least significant. The largest change in the signal is found for the HDPE liner. This characteristic influence can be explained by the shift of the neutral axis of the hybrid plate with respect to the medial plane. This affects the bending stiffness, which turns into different amplitudes of the excited  $A_0$ -mode. Similarly, in-plane stiffness is governed by the averaged elastic properties of both constituents. The closest match to the  $C_{11}$  coefficient of 154.0 GPa of the T800/913 is found for titanium having an

elastic modulus of 110.2 GPa. Stronger deviations are found for aluminum with 70.0 GPa and HDPE with only 1.1 GPa, respectively. This mismatch of elastic properties translates into the severity of the deviations to the signal of a pure CFRP plate.

#### **4.4 Stacking Sequence**

Since realistic fiber reinforced structures are rarely composed of unidirectional oriented plies, the next step is the investigation of stacking sequences typically found for CFRP. For this assessment, the liner material is chosen as aluminum and the thickness is kept constant at 0.125 mm with a composite thickness of 0.875 mm. It is worth noting, that a larger number of plies is hard to realize in practice keeping the total thickness constant at 1 mm. We decided to neglect this problem and keep the thickness constant for the numerical modeling, since this is the only way to investigate the influence of ply angles independent of the influence of plate thickness.

Figure 9 shows the signals detected on the top surface (composite side) for a unidirectional layup  $[0]_{\text{sym}}$  and stacking sequences of  $[0/90]_{\text{sym}}$  and  $[0/45/-45/90]_{\text{sym}}$ . For actual individual ply thicknesses between 100  $\mu\text{m}$  and 400  $\mu\text{m}$ , it is evident that these stacking sequences would result in a total laminate thickness above 1.0 mm for most cases.

Similar to the results of previous studies on signal propagation in pure CFRP [16, 21] a strong influence of the stacking sequence on the simulated Lamb-waves is observed. This is due to the strong dependence of the anisotropic elastic properties on the chosen stacking sequence, which governs the shape of  $S_0$ -mode and  $A_0$ -mode.

#### **4.5 Pressure Vessel**

To demonstrate the applicability of the modeling approach to more complex geometries than plates, we choose the geometry of a small pressure vessel with outer diameter of 192 mm as shown in figure 2. The inner part of the vessel is chosen as 0.125 mm thick aluminum structure. In the cylindrical part of the vessel, the stacking sequence  $[16_2/-16_2/90_3]_{\text{sym}}$  is chosen to emulate a configuration typical for a hoop wrapped reinforced pressure vessel. Similar to the investigations

above, the total thickness of the composite was chosen to be 0.875 mm applied on a 0.125 mm thick aluminum vessel.

The calculated wave-field on the composite outer surface for a dipole source buried within the vessel (see figure 2) is shown in figures 10-a to 10-c in gray-scale plots of the calculated out-of-plane component at 10  $\mu$ s, 20  $\mu$ s and 40  $\mu$ s after signal excitation. As seen in the figure, the spreading of the wave-field is complex in nature and governed by the anisotropy of the elastic properties. Within the calculated first 50  $\mu$ s the signal propagates throughout the whole structure with reflections of the  $S_0$ -mode occurring at the aluminum dome region of the pressure vessel. These reflections can cause a significant contribution to the overall signal as seen in the simulated signal obtained at 100 mm distance for  $0^\circ$  propagation angle. Due to the symmetry conditions, the circumferential path of signal propagation is also taken into account in the model. This causes a signal arrival from the opposite path of the circumferential signal on the composite surface after 75  $\mu$ s as seen in figure 10-d.

## **5 CONCLUSIONS**

Within the present study it was demonstrated that the proposed finite element method can accurately calculate Lamb-wave propagation in hybrid materials composed of isotropic and anisotropic media. It was found that Lamb-wave propagation can occur as motion of the complete multi-layered plate, which can be superimposed by guided waves within the individual layers. The occurrence of propagation of signals in individual layers was found to increase with plate thickness. For the case of the CFRP studied here, it was demonstrated, that acoustic emission signals originating from buried dipole sources are strongly affected by the material properties of the multi-layered plates. A strong anisotropy in the material properties influences the directional dependency of signal propagation stronger than for example those resulting from quasi-isotropic stacking sequences. Thin metallic structures, like those typically used as liner materials, had a small influence on signal propagation. The mismatch between the elastic properties of the liner and the composite can cause shifts of the amplitude ratio between  $S_0$ - and  $A_0$ -mode for the same type of source.

As a representative structure for practical health monitoring applications, a small pressure vessel was investigated. Given a sufficient amount of computational capacity, finite element simulation of such structures is a feasible tool to study wave propagation in complex geometries. For the pressure vessel studied, this allows prediction of circumferential wave arrivals or incident reflections.

## Literature

1. Wevers M and Lambrighs K. Applications of Acoustic Emission for SHM: A Review, Encyclopedia of Structural Health Monitoring, John Wiley & Sons, 2009.
2. Bohse J, Mair GW and Novak P. Acoustic Emission Testing of High-Pressure Composite Cylinders. *Adv. Mater. Res.* 2006;13-14:267-272.
3. Downs KS and Hamstad MA. Wave Propagation Effects Relative to AE Source Distinction of Wideband AE Signals from a Composite Pressure Vessel. *J. Acoustic Emission* 1996;14(3-4):61-73.
4. Downs KS and Hamstad MA. Acoustic Emission from Depressurization to Detect/Evaluate Significance of Impact Damage to Graphite/Epoxy Pressure Vessels. *J. Compos. Mater.* 1998;32(3):258-307.
5. Whittaker JW, Brosey WD, Hamstad MA. Correlation of Felicity Ratio and Strength Behavior of Impact-Damaged Spherical Composite Test Specimens. In: Proceedings of the Third International Symposium on Acoustic Emission from Composites, Paris, 1989. p. 160-167
6. Gorman MR. Burst Prediction by Acoustic Emission in Filament-Wound Pressure Vessels, *J. Acoustic Emission* 1990;9(2):131-139.
7. Lamb H. On Waves in an Elastic Plate. *P. Roy. Soc. Lond. A. Mat.* 1917;93:114-128.
8. Gorman MR. Plate Wave Acoustic Emission. *J. Acoust. Soc. Am.* 1991;90(1):358-364.
9. Prosser WH. Advanced AE Techniques in Composite Materials Research. *J. Acoustic Emission* 1996;14(3-4):01-11.
10. Anastassopoulos AA and Philippidis TP. Clustering Methodology for the Evaluation of Acoustic Emission from Composites. *J. Acoustic Emission* 1995;13:11-21.
11. Atitivavas N, Pothisiri T and Fowler TJ. Identification of Fiber-reinforced Plastic Failure Mechanisms from Acoustic Emission Data using Neural Networks. *J. Compos. Mater.* 2006;40(3):193-226.
12. Marec A, Thomas J-H and Guerjouma R. Damage characterization of polymer-based composite materials: Multivariable analysis and wavelet transform for clustering acoustic emission data. *Mech. Syst. Signal Pr.* 2006;22:1441-1464.
13. Ramirez-Jimenez C-R, Papadakis N, Reynolds N, Gan T, Purnell P and Pharaoh M. Identification of failure modes in glass/polypropylene composites by means of the primary frequency content of the acoustic emission event. *Compos. Sci. Technol.* 2004;64:1819-1827.

14. Huguet S, Godin N, Gaertner R, Salmon L and Villard D. Use of acoustic emission to identify damage modes in glass fibre reinforced polyester. *Compos. Sci. Technol.* 2002;62:1433-1444.
15. Sause MGR, Gribov A, Unwin AR and Horn S. Pattern recognition approach to identify natural clusters of acoustic emission signals. *Pattern. Recogn. Lett.* 2012;33(1):17-23.
16. Sause MGR. Identification of failure mechanisms in hybrid materials utilizing pattern recognition techniques applied to acoustic emission signals, PhD Dissertation, Augsburg University, Augsburg, Germany, 2010.
17. de-Oliveira R, Marques AT. Health monitoring of FRP using acoustic emission and artificial neural networks. *Comput. Struct.* 2008;86(3–5):367-373.
18. Aggelis DG, Matikas TE. Effect of plate wave dispersion on the acoustic emission parameters in metals. *Comput. Struct.* 2012;98–99:17-22.
19. Castaings M, Bacon C, Hosten B and Predoi MV. Finite element predictions for the dynamic response of thermo-viscoelastic material structures. *J. Acoust. Soc. Am.* 2004;115(3):1125-1133.
20. Moser F, Jacobs LJ and Qu J. Modeling elastic wave propagation in waveguides with the finite element method. *NDT & E International* 1999;32(4):225-234.
21. Sause MGR and Horn S. Simulation of acoustic emission in planar carbon fiber reinforced plastic specimens. *J. Nondestruct. Eval.* 2010;29(2):123-142.
22. Sause MGR and Horn S. Simulation of Lamb Wave Excitation for Different Elastic Properties and Acoustic Emission Source Geometries. *J. Acoustic Emission* 2010;28:109-121.
23. Thompson WT. Transmission of elastic waves through a stratified solid medium. *J. Appl. Phys.* 1950;21:89-93.
24. Haskell NA. The dispersion of surface waves on multilayered media. *B. Seismol. Soc. Am.* 1950;43:17-34.
25. Lowe MJS. Matrix techniques for modeling ultrasonic waves in multilayered media. *IEEE T. Ultrason. Ferr.* 1995;42(4):525-542.
26. Kundu T and Mal AK. Elastic Waves in a Multilayered Solid Due to a Point Source. *Wave Motion* 1985;7:459-471.
27. Sause MGR, Hamstad MA and Horn S. Finite Element Modeling of Conical Acoustic Emission Sensors and Corresponding Experiments. *Sensors & Actuators: A Physical* 2012;184:64-71.
28. Sause MGR. Investigation of Pencil Lead Breaks as Acoustic Emission Sources. *J. Acoustic Emission* 2011;29:184-196.
29. Gary J and Hamstad MA. On the Far-field Structure of Waves Generated by a Pencil Lead Break on a Thin Plate. *J. Acoustic Emission* 1994;12(3-4):157-170.
30. Sause MGR, Schultheiß D, Horn S. Acoustic emission investigation of coating fracture and delamination in hybrid carbon fiber reinforced plastic structures. *J. Acoustic Emission* 2008;26:01-13.
31. Sause MGR, Haider F, Horn S. Quantification of metallic coating failure on carbon fiber reinforced plastics using acoustic emission. *Surf. Coat. Technol.* 2009;204:300-308.



Property	AlMg3	Ti-6Al-4V	HDPE	T800/913 (UD)
Density $\rho$ [kg/m <sup>3</sup> ]	2660	4430	959	1550
Elastic Modulus [GPa]	70.0	110.2	1.1	$C_{11} = 154.0$ $C_{22} = C_{33} = 9.5$ $C_{12} = C_{13} = 3.7$ $C_{23} = 5.2$ $C_{44} = 2.5$ $C_{55} = C_{66} = 4.2$
Poisson ratio	0.33	0.40	0.38	-

**Tab.1:** Elastic properties of the materials used in finite element modeling.

Property	Al	Al 0.5 / CFRP 0.5	Al 0.25 / CFRP 0.75	Al 0.125 / CFRP 0.875	CFRP
$S_0$ -velocity [m/s] (simulation)	6289	8772	10101	10872	11403
$A_0$ -velocity [m/s] (simulation)	3165	2551	2049	1799	1799
$S_0$ -velocity [m/s] (rule of mixture)	-	8846	10125	10764	-

**Tab.2:** Calculated sound velocities of two-layer system.

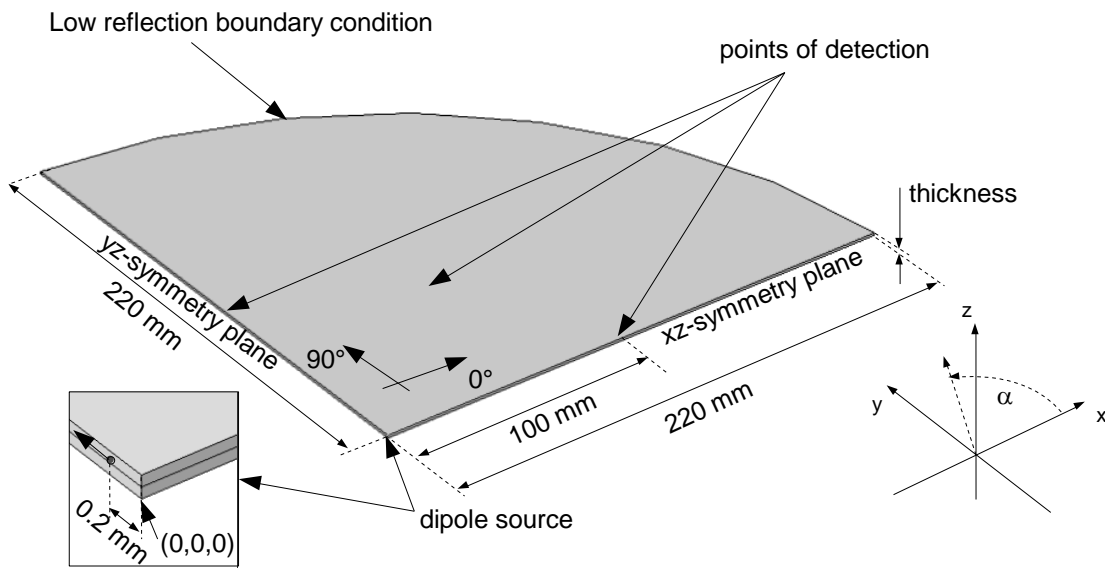


**Fig. 1:** 3-dimensional model setup used for simulation of Lamb-wave propagation in hybrid multi-layered plates.

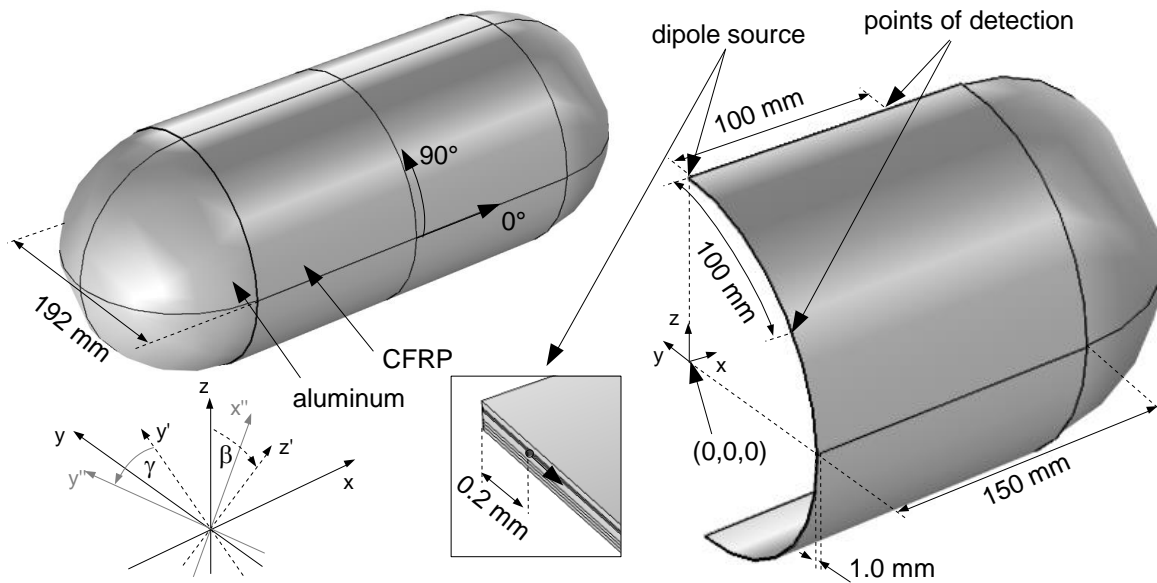


**Fig. 2:** 3-dimensional model of pressure vessel for simulation of Lamb-wave propagation (left) and quarter-volume model actually used for the simulation (right).

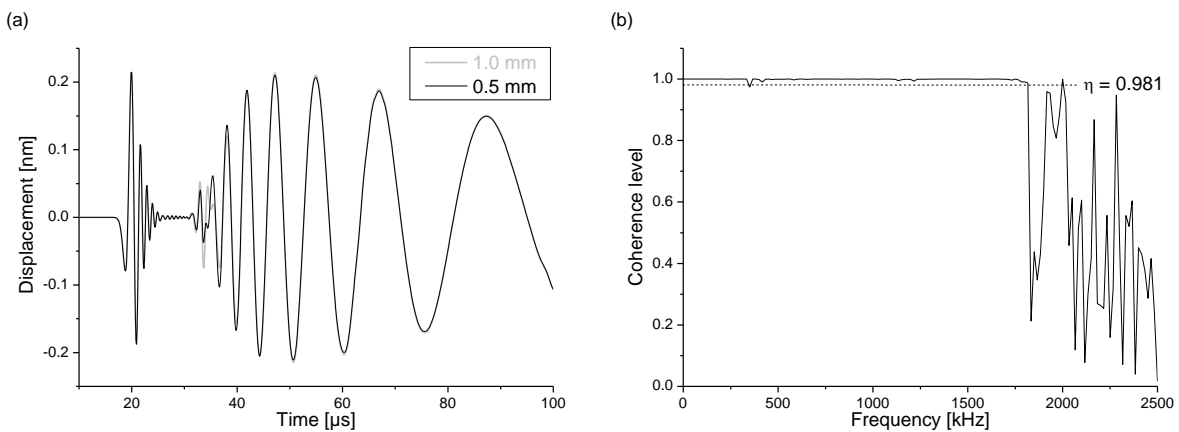


**Fig. 3:** Comparison of signals with 1 mm mesh resolution and 0.5 mm mesh resolution (a). Calculated coherence level of both signals (b).

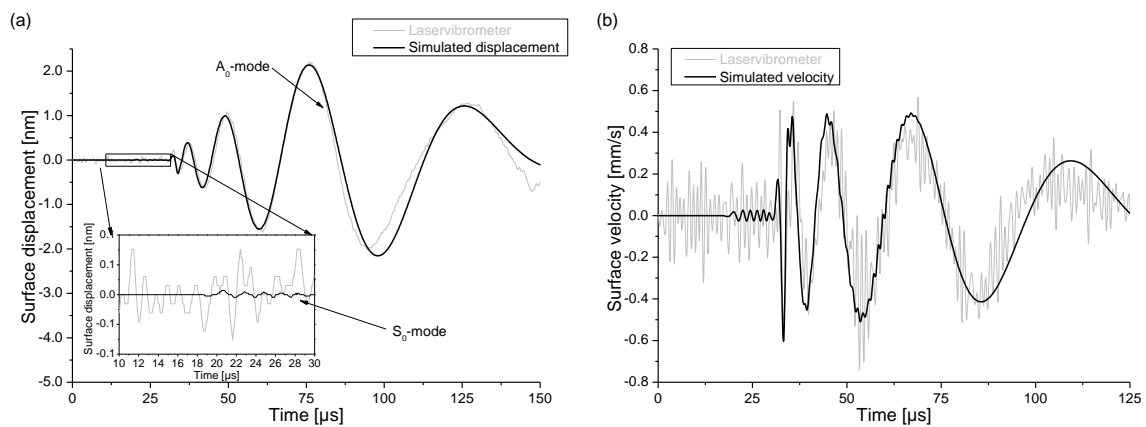


**Fig. 4:** Comparison of simulation results and measurement of out-of-plane displacement (a) and out-of-plane velocity (b) using Laservibrometer for signal of pencil lead breakage at distance of 100 mm.

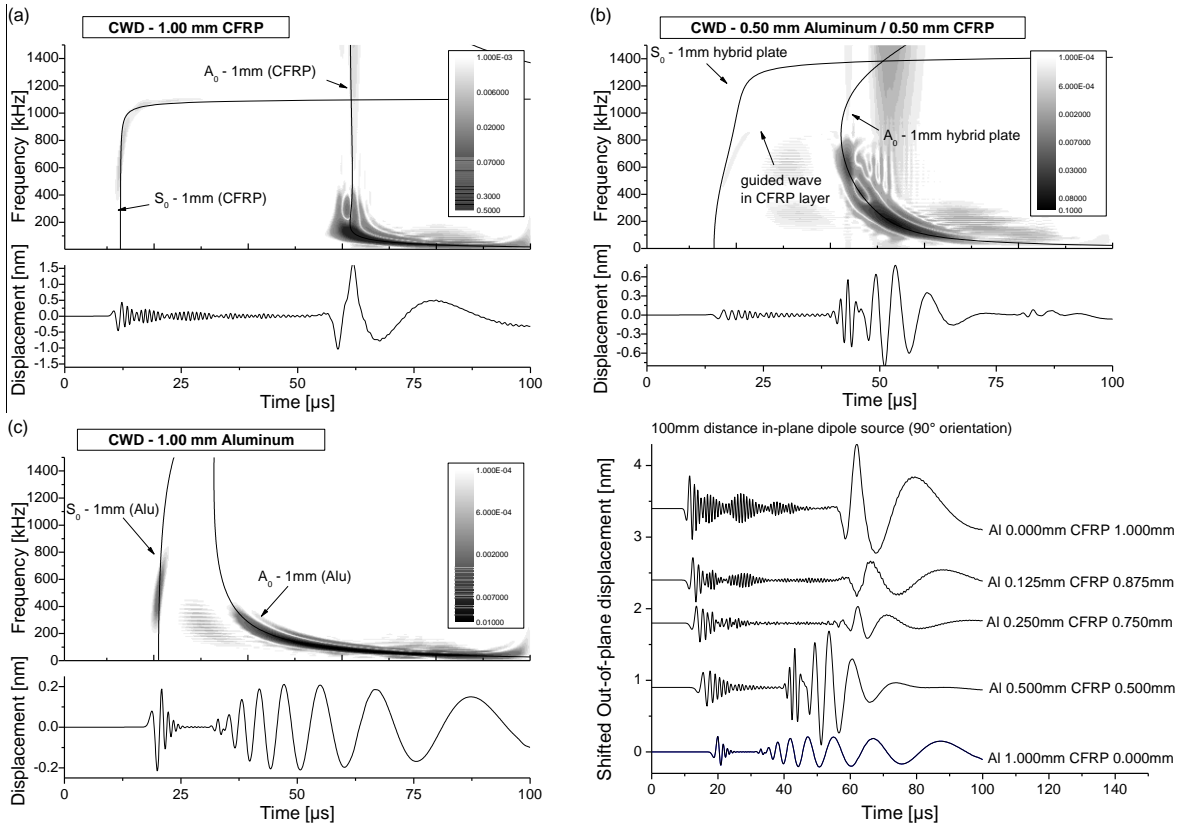


**Fig. 5:** Simulated signals of AE dipole source in two-layer system with varying thickness ratio between aluminum and T800/913 unidirectional CFRP obtained at 100 mm distance for 90° propagation angle. Figures (a) to (c) show Choi-Williams distribution (logarithmic scale) of selected configurations with superimposed dispersion curves, figure (d) shows comparison of all configurations.

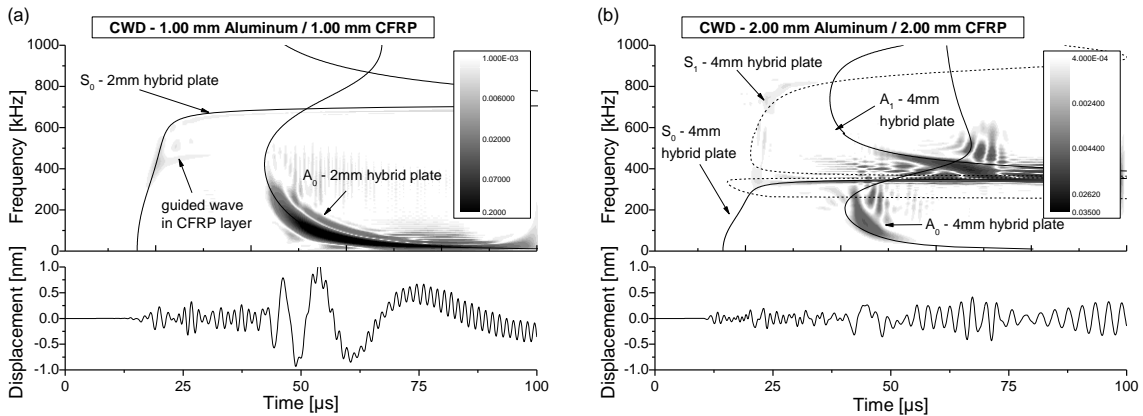


**Fig. 6:** Choi-Williams distribution (logarithmic scale) of simulated signals of AE dipole source in two-layer system with total thickness of 2.00 mm (a) and 4.00 mm (b) obtained at 100 mm distance for 90° propagation angle.

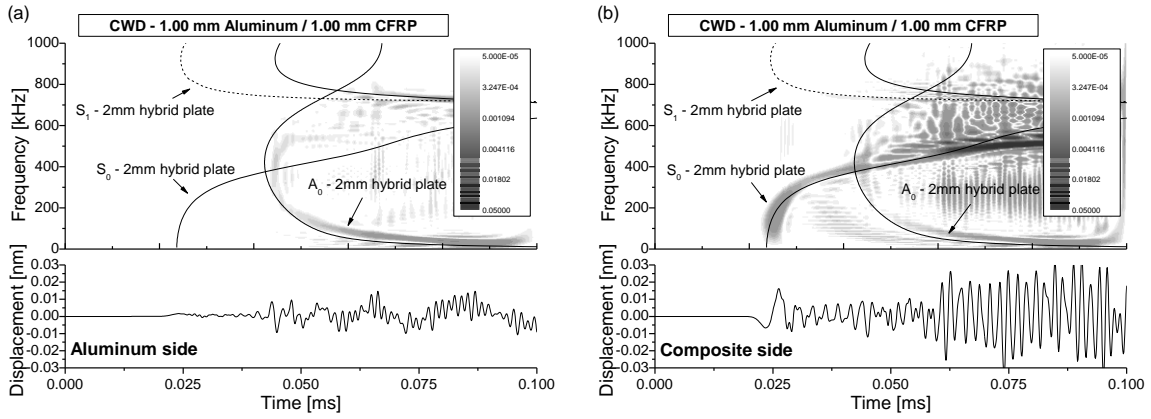


**Fig. 7:** Choi-Williams distribution (logarithmic scale) of simulated signals of AE dipole source in two-layer system with total thickness of 2.00 mm obtained at 100 mm distance for  $0^\circ$  propagation angle on aluminum side (a) and composite side (b).

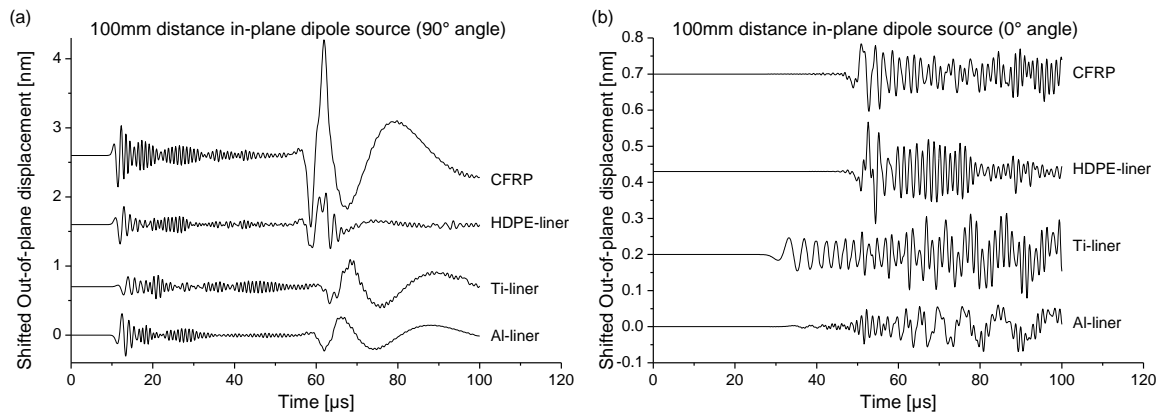


**Fig. 8:** Simulated signals of AE dipole source in two-layer system with various elastic properties of liner material obtained at 100 mm distance for  $90^\circ$  and  $0^\circ$  propagation angle.

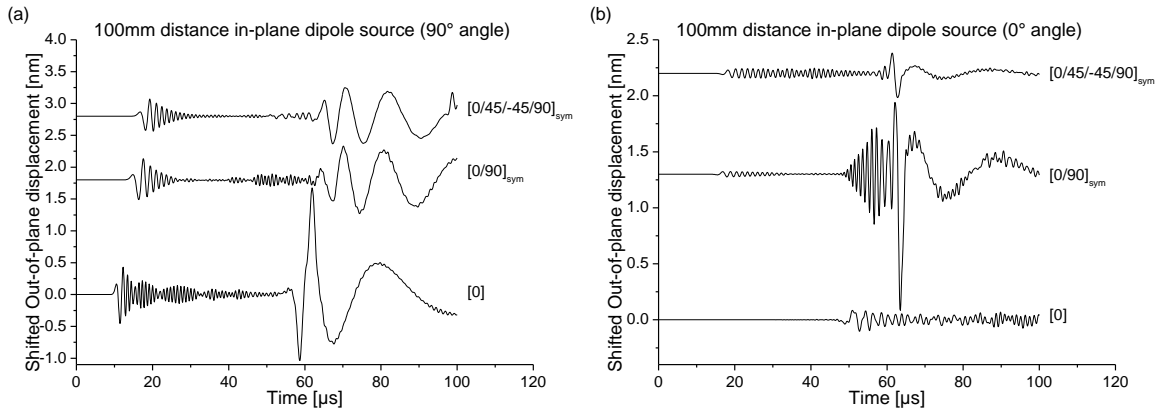


**Fig. 9:** Simulated signals of AE dipole source in two-layer system of T800/913 CFRP with various stacking sequences and aluminum liner material obtained at 100 mm distance for  $0^\circ$  and  $90^\circ$  propagation angle.

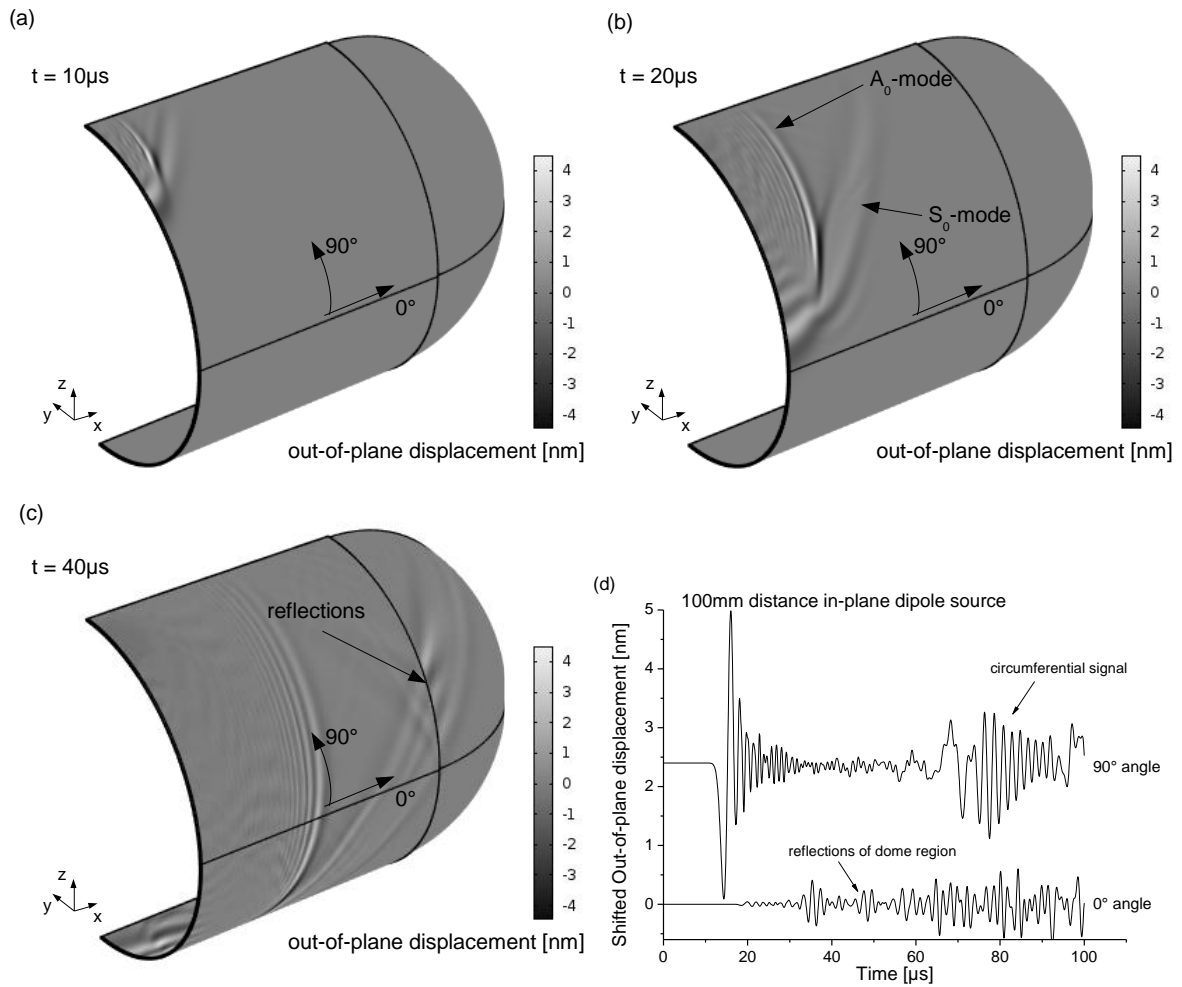


**Fig. 10:** Calculated out-of-plane component after signal excitation at  $t = 10\mu\text{s}$  (a),  $t = 20\mu\text{s}$  (b) and  $t = 40\mu\text{s}$  (c). Simulated signals obtained at 100 mm distance for  $0^\circ$  and  $90^\circ$  propagation angle (d).